Optofluidic tunable microlens by manipulating the liquid meniscus using a flared microfluidic structure

Xiaole Mao,[1,2] Zackary I. Stratton,[1] Ahmad Ahsan Nawaz,[1] Sz-Chin Steven Lin,[1] and Tony Jun Huang[1,2,a)]
[1]*Department of Engineering Science and Mechanics, The Pennsylvania State University, University Park, Pennsylvania 16802, USA*
[2]*Department of Bioengineering, The Pennsylvania State University, University Park, Pennsylvania 16802, USA*

(Received 19 August 2010; accepted 17 September 2010; published online 30 December 2010)

We have designed, demonstrated, and characterized a simple, novel in-plane tunable optofluidic microlens. The microlens is realized by utilizing the interface properties between two different fluids: $CaCl_2$ solution and air. A constant contact angle of ~90° is the pivotal factor resulting in the outward bowing and convex shape of the $CaCl_2$ solution-air interface. The contact angle at the $CaCl_2$ solution-air interface is maintained by a flared structure in the polydimethylsiloxane channel. The resulting bowing interface, coupled with the refractive index difference between the two fluids, results in effective in-plane focusing. The versatility of such a design is confirmed by characterizing the intensity of a traced beam experimentally and comparing the observed focal points with those obtained via ray-tracing simulations. With the radius of curvature conveniently controlled via fluid injection, the resulting microlens has a readily tunable focal length. This ease of operation, outstandingly low fluid usage, large range tunable focal length, and in-plane focusing ability make this lens suitable for many potential lab-on-a-chip applications such as particle manipulation, flow cytometry, and in-plane optical trapping. © *2010 American Institute of Physics.* [doi:10.1063/1.3497934]

I. INTRODUCTION

The integration of optics with on-chip microfluidic devices is of great interest in many applications, especially biological assays such as biodetection,[1–8] imaging,[9–12] and particle manipulation.[13–20] Consolidation of optics with microfluidics is difficult and requires meticulous research because of the delicacy and complexity of such devices. Optofluidics[21,22] is a versatile branch of microfluidics that benefits from the convergence of these two fields (i.e., optics and microfluidics), with the advantage of greatly increased simplicity in the fabrication of micro-optical components (e.g., lens, waveguide). In the case of lenses, many methods have been developed and demonstrated that can focus light out of the plane of the substrate of the device.[23–30] A common approach to create an out-of-plane lens is to mechanically alter the curvature of an elastic polydimethylsiloxane (PDMS) membrane by mechanical actuation.[23–28] Additionally, a liquid meniscus can be modulated through various methods such as electrowetting or responsive hydrogel.[29,30] Such out-of-plane lenses, with their optical axis perpendicular to the substrate, present alignment difficulties, thus restricting their use and diminishing potential applications.

In most applications, in-plane optofluidic lenses are more advantageous as they offer a wider range of applications and reduce the setup complexity. In-plane lenses have also been developed and reported.[31–34] These lenses are generally PDMS chambers filled with liquid,[31,32] where the curvature of surfaces results in convergence of the incident light. The focal length can be adjusted

a)Author to whom correspondence should be addressed. Electronic mail: junhuang@psu.edu.

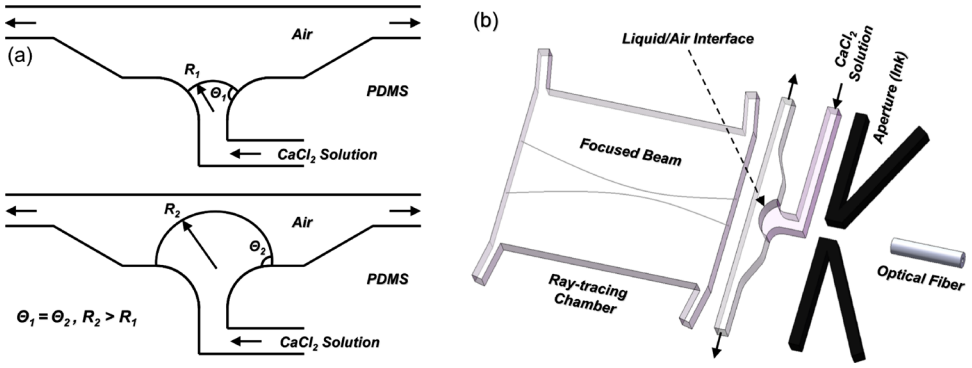

FIG. 1. (a) Principle of the meniscus lens. The device includes a bowed structure. When the $CaCl_2$ solution is injected, the fluid advances through the flange while the contact angle remains constant. The unchanged contact angle with the fluidic volume change results in a varied meniscus radius. The varied meniscus radius can be used to focus light. (b) A schematic of the lens, including an optical fiber, aperture (dark ink channel) to block the undesired light, bubble-tuning channel, and ray-tracing chamber that is filled with fluorescent dye for visualizing the focused beam profile.

by changing the refractive index of filling solution. The disadvantage of these methods is that they require a variety of filling solutions with different refractive indices to achieve multiple focal positions.

Another approach working toward tunability of in-plane optofluidic lenses involves manipulation of virtual interfaces between two laminarly flowing miscible fluids (such as water-$CaCl_2$ Solutions). Due to the laminar flow, the virtual interface between such fluids is extremely smooth and provides an excellent optical surface, thus minimizing certain optical aberrations. This was demonstrated in a hydrodynamic cylindrical lens,[33] where coinjected miscible liquids of different refractive indices were made to pass through a curved channel, causing one liquid to bow into the other, thus forming a hydrodynamically controlled in-plane lens. Another lens, utilizing a similar concept, is a liquid-core liquid-cladding (L^2) lens.[34,35] In this lens a laminar flow of three liquid streams was demonstrated to show a tunable focal length of up to 6 mm; in this case the core and cladding were manipulated by changing the relative flow rate of the streams. The core stream in this case was of higher refractive index and was sandwiched between two low refractive index streams (cladding). These methods based on liquid-liquid interface are more flexible in terms of variable light focusing, but constant injection of flows at high and low rates is needed. Another technique used a liquid gradient refractive index lens,[36,37] where the diffusion of a coinjected solute ($CaCl_2$) in de-ionized (DI) water was shown to exhibit a hyperbolic secant refractive index profile and not only focus light, but also bend the light propagation. This method requires a much lower flow rate for operation; yet the constant need of flow injection still presents a challenge.

In this work, we used a standard soft lithography technique to develop an in-plane, tunable microlens based on liquid meniscus. We took advantage of the constant contact angle between the $CaCl_2$ solution-air interface at the PDMS walls to change the radius of curvature of the liquid meniscus which acts as a convex lens. We have demonstrated the control of the focal length by simply changing the position of the liquid meniscus to alter the radius of curvature of the $CaCl_2$ solution-air interface. This in-plane tunable microlens, when compared with the previously introduced methods, has advantages such as ease of operation (no constant flow is needed), low fluid usage, and flexible tuning capability.

II. WORKING MECHANISM

The working mechanism of the microlens is illustrated in Fig. 1. The working principle takes advantage of the constant contact angle created between the $CaCl_2$ solution-air interface and flared PDMS channel walls. We observed that the PDMS is hydrophobic and has a contact angle of $\sim 90°$ with $5M$ $CaCl_2$ solution. The flared PDMS channel walls cause the $CaCl_2$ solution-air interface to be curved outward, thus forming the convex shape of the droplet for light focusing.

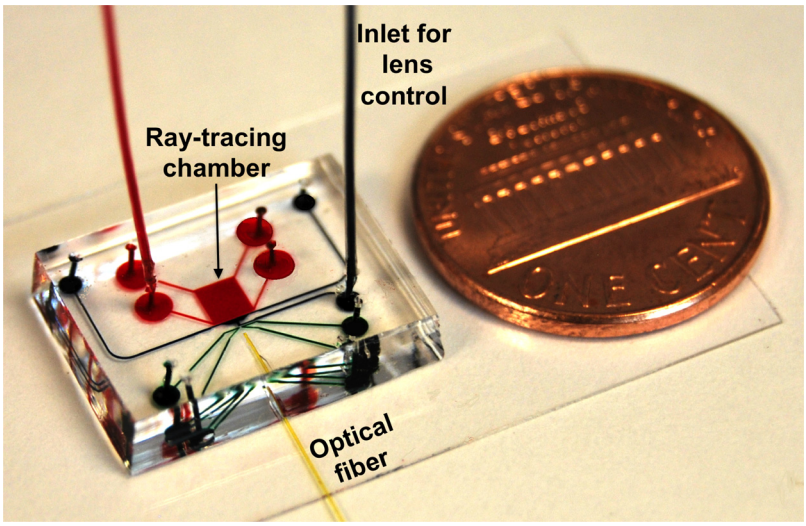

FIG. 2. Optical image of the assembled lens device.

$CaCl_2$ solution is manually introduced through a syringe into an inlet channel. The increase in the size of the droplet pushes the air out of the exit channels, as shown by the arrows in Fig. 1(a). As the volume of $CaCl_2$ solution increases, the radius of curvature of the $CaCl_2$ solution-air interface increases while the contact angle remains the same ($\theta_2 = \theta_1$).

The refractive indices of $5M$ $CaCl_2$ solution, air, and PDMS are ~1.445, ~1, and ~1.412, respectively. The ray-tracing chamber was filled with rhodamine fluorescent dye and $3.5M$ $CaCl_2$ solution so as to match the refractive index of PDMS, thus reducing the light loss caused by reflection and scattering at the walls of the ray-tracing chamber. The refractive index difference between $5M$ $CaCl_2$ solution and air is ~0.445, which is large enough to be used as a converging lens and will subsequently follow conventional lens operation.[33] As shown in Fig. 1(b), light is introduced into the device by an optical fiber and focused in the ray-tracing chamber by the curvature of the meniscus. The aperture inks are designed to absorb unwanted light. Increasing the volume of the $5M$ $CaCl_2$ solution results in an increase in the radius of the meniscus, and as such, shifts the focus to a farther position in the ray-tracing chamber.

III. DEVICE FABRICATION AND SETUP

A three-dimensional schematic of the proposed microlens design is illustrated in Fig. 1(b). Standard soft lithography and mold-replica procedures were used to fabricate microfluidic channels from PDMS.[38] Initially, a silicon wafer was patterned with the desired channel features by deep reactive ion etching (DRIE, Adixen, Hingham, MA) with an etch depth of 155 μm. After DRIE treatment, the silicon mold contains the positive impression of the intended design features. The master mold is subsequently silanized by coating it with vapors of 1H, 1H, 2H, 2H-perfluorooctyltrichlorosilane (Sigma Aldrich) in order to reduce its surface energy; such a treatment makes the surface of the silicon mold hydrophobic, thus preventing the PDMS channels from distorting or deforming during the detachment process. This practice significantly enhances the quality of the channel walls, which in turn improves the quality of the microlens results. Sylgard™ 184 Silicone Elastomer base and Sylgard™ 184 Silicone Elastomer curing agent (Dow Corning) were then mixed in a 10:1 weight ratio and applied to the silicon mold; this was followed by degassing in a vacuum chamber. A cure at 70 °C for approximately 30 min followed the degassing. Once cured and peeled off, the inlets and outlets were drilled in the PDMS channel, after which the channel was sealed to a glass slide. Polyethylene tubes were then inserted into the inlets and outlets to connect the device to syringe pumps (KDS 210, KD scientific, Holliston, MA). The image of the assembled lens device is shown in Fig. 2.

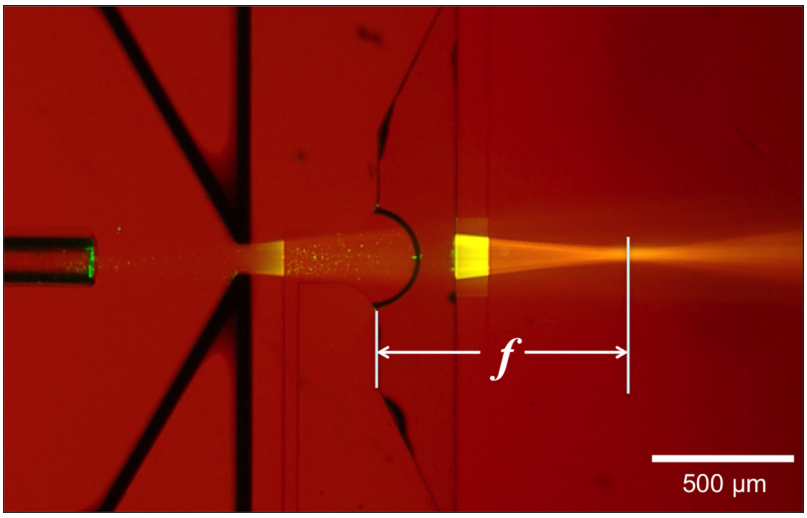

FIG. 3. Microscopic image of the lens in operation: the laser light emitted from the optical fiber being focused after passing through meniscus lens. The path of the light was highlighted due to fluorescent emission of the dye in ray-tracing chamber.

Incident light was supplied by a green diode laser (532 nm) coupled into an optical fiber Ocean Optics, NA = 0.22 ± 0.02 (NA denotes numerical aperture), core and outer diameters are 50 and 155 μm, respectively. The optical fiber was inserted into a channel (155 μm × 155 μm) in the PDMS to maintain its position such that the axis of the fiber was aligned along the optical axis of the PDMS lens. We used black ink channels to form a slit, as shown in Fig. 3, which would act as an aperture. Since the optical center of the lens changes with the radius of the meniscus, we have taken the channel edge to be the reference in order to determine and compare the measured and the simulated focal length f, as illustrated in Fig. 3. In order to visualize the light rays, 3.5M $CaCl_2$ solution rhodamine fluorescent dye was injected into the ray-tracing chamber. The intensity of the dye fluorescence is proportional to the intensity of incident light. The concentration of the dye in the ray-tracing chamber was kept sufficiently low so that the incident light could propagate through the liquid without being significantly attenuated, while the intensity of the incident light was sufficiently low (5 mW) so as to avoid photobleaching of the dye during the experiments. The device operation was observed through an inverted fluorescent optical microscope (Nikon TE 2000U), and optical images were taken using a charge coupled device camera (CoolSNAP HQ2, Photometrics, Tucson, AZ) and a Nikon color digital camera mounted on the front viewport of the microscope.

IV. RESULTS AND DISCUSSION

A. Experimental results

The surface properties affect the contact angle, and together with the chamber geometry, determine the curvature of the air-liquid interface (liquid lens surface). In this work we used a flared structure maintaining a constant contact angle (which is approximately 90°) to realize the change in lens curvature and hence the focal point. The curvature of the $CaCl_2$ solution-air interface was manually controlled via 1 ml syringe through the inlet that introduces the 5M $CaCl_2$ into the channel. Initially, the flow injection was paused as curved $CaCl_2$ solution-air interface approached the bowed edges of the channel. In such a case the beam of light that emerges from the microlens is parallel to the optical axis and the focal point is indistinguishable. As the curved $CaCl_2$ solution-air interface proceeds and reaches the bowed edges of the channel, the interface curvature is formed, as is shown in Fig. 4(a), thus causing the incident laser light to focus just beyond the nearest wall of the ray-tracing chamber. It is somewhat difficult to observe the ray-tracing chamber walls since the 3.5M $CaCl_2$ solution has a refractive index that matches well with

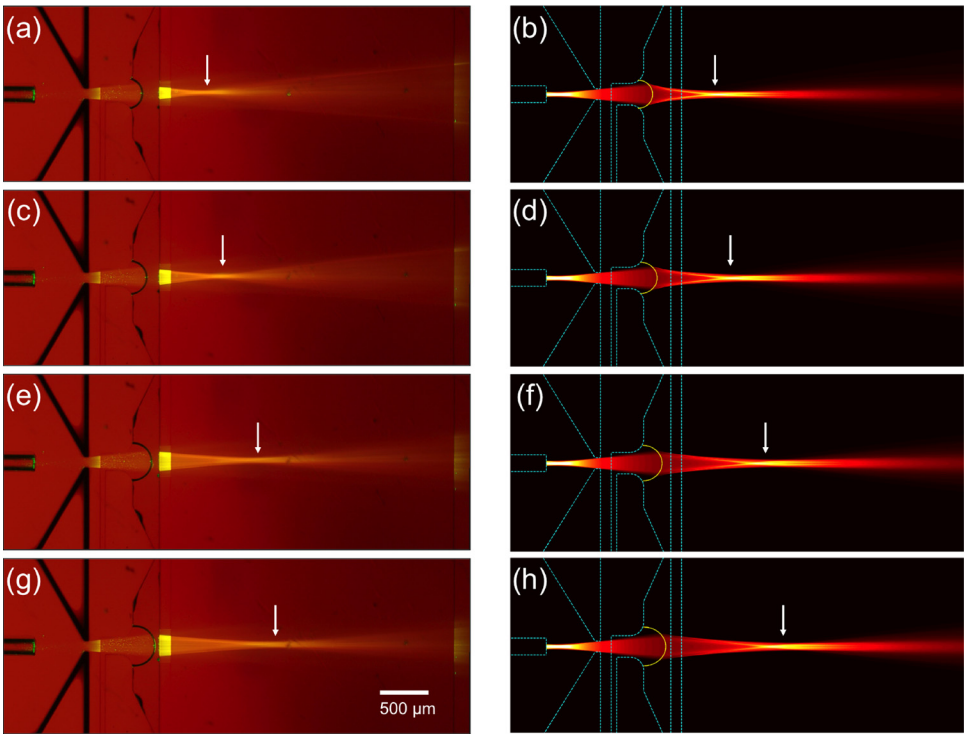

FIG. 4. [(a), (c), (e), and (g)] Ray-tracing experiments to characterize the variable focal length. [(b), (d), (f), and (h)] The simulation results corresponding to their complementary experimental results.

that of PDMS (~1.412). Further injection of 5*M* $CaCl_2$ solution at the lens inlet results in a subsequent increase in the volume of the $CaCl_2$ solution, and hence the radius of curvature of the $CaCl_2$ solution-air interface and the focal length of the lens. In this design the channel geometry, refractive index of the solution, and contact angle of $CaCl_2$ solution on PDMS surface are all fixed; only the width of the bowed chamber channel can determine the tuning range of the lens. As the intensity of the fluorescence emission is proportional to the intensity of the incident laser light, we used an image-processing software package IMAGEJ to determine the focal point of the lens by taking the maximum florescent intensity as the focal point.[34,36] The maximum tunable range of the lens could then be determined and was found to be approximately 500 μm. We believe that this tuning range should be sufficient for most lab-on-a-chip applications considering the size of a typical microfluidic channel to be ~100 μm. However, the channel geometry and dimension can be further optimized to satisfy the requirement of various applications. The white arrows in Figs. 4(a), 4(c), 4(e), and 4(g) indicate the points of maximum intensity of the light under each lens condition. It can therefore be observed that, in accordance with conventional lens theory, the focal point shifts away from the lens as the radius of curvature increases. As the curvature of the lens surface is primarily determined by the contact angle and chamber geometry, we believe that the repeatability of the lens is mainly dependent upon the repeatability of channel fabrication (e.g., PMDS surface properties and the chamber structure) and material preparation (e.g., $CaCl_2$ concentration). Both channel fabrication and material preparation processes can be conveniently standardized which can help achieve a high repeatability. Throughout our study we have observed a very consistent lens performance. The resolution of the lens is dependent upon the precision of the $CaCl_2$ solution injection. In current work, the injection of $CaCl_2$ solution was carried out manually. If necessary, a precision pump (with a resolution of nanoliter) can be used, which translates to a lens adjustment resolution of <1 μm. In our experiments we have also observed a high time-stability of the lens. Due to the setup of the liquid lens (enclosed channel with a large adjacent reservoir), the evaporation of the liquid was negligible. In our experiments we were able to

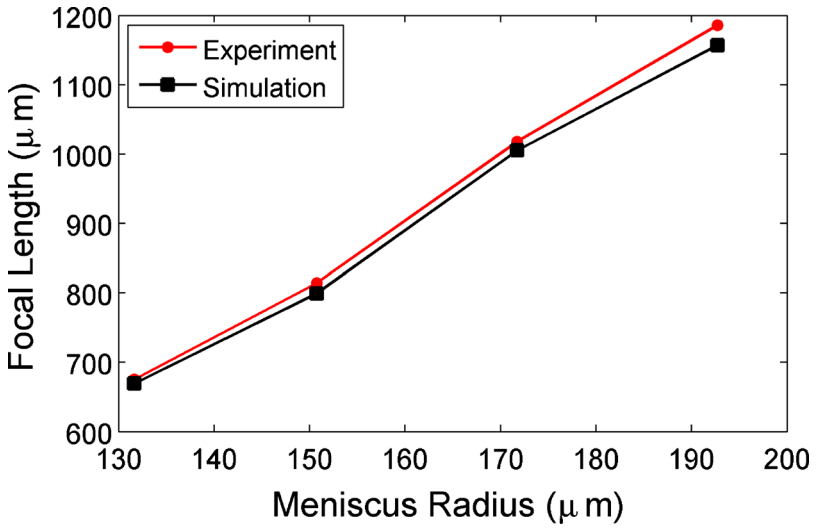

FIG. 5. Comparison between experimental and simulated results illustrates the meniscus radius as a function of focal length.

observe a stable light focusing for at least 4 h. Compared to our previous work on tunable microlens based on hydraulic pressure activated microbubble,[39] the current design represents a further improvement in fluid consumption as the lens does not require a constant stream of flows, and the focal position is self-sustained (the focal position does not change when flow injection is ceased), whereas in our previous work[39] the constant pumping of fluid is needed to maintain the hydraulic pressure to keep the microbubble curvature and the focal position constant.

B. Ray-tracing simulation

In order to supplement the experimental work, we performed ray-tracing simulations using MATLAB. The simulation results are shown in Figs. 4(b), 4(d), 4(f), and 4(h) juxtaposed with their corresponding experimental photographs. The ray-tracing simulation results are depicted by arrows in Figs. 4(b), 4(d), 4(f), and 4(h). In the simulations, as in the experimental results, the point of maximum intensity is taken to be the focal point. As expected, since the fluid injection causes the $CaCl_2$ solution-air interface to proceed outward toward the flared end of the channel, the corresponding simulated focal lengths increase as a result of the increase in radius of curvature.

In order to study the correlation between the experimentally observed and the simulated focal lengths, the radius of curvature was plotted as a function of the focal length (Fig. 5). It is evident that the simulated and the experimental results are in good correlation with one another. However, at higher radius of curvature, a slight deviation in the experimental results from the simulated results was observed. The main reason for this observation appears to be the optical aberration caused by the nonuniform radius of curvature at higher meniscus radius. Nevertheless, the largest discrepancy between the experimentally measured and simulated focal length is within 2.5%. In this aspect, the microlens we have developed is highly predictable, reliable, and pragmatic. It also boasts other advantages such as large tunable focal range, ease of operation, low fluid usage, and in-plane focusing ability.

V. CONCLUSION

We have successfully demonstrated a tunable, in-plane microlens by manipulating the liquid meniscus using a flared microfluidic structure. Our experimental results are supported by simulated data using a ray-tracing method. The microlens uses a meniscus created by a $5M$ $CaCl_2$ solution-air interface. By manually changing the volume of the $5M$ $CaCl_2$ solution meniscus, we have shown that the proposed in-plane microlens has a tunable focal length ranging up to

500 μm. This lens can be conveniently fabricated with the soft lithography technique. Moreover, being an in-plane microlens, it provides significant advantages over out-of-plane lenses through potential integration with many other on-chip components. Another benefit offered by such a technique is the extremely low usage of fluids in order to control the focal length of the lens. In summary, such a microlens provides excellent performance in terms of control of the focal length; therefore, it could be valuable in many on-chip optical applications such as in-plane optical tweezers, flow cytometry, and particle manipulation.

ACKNOWLEDGMENTS

This research was supported by NIH Director's New Innovator Award (1DP2PD007209-01), Department of Agriculture (USDA/NRI), National Science Foundation, Air Force Office of Scientific Research (AFOSR), and the Penn State Center for Nanoscale Science (MRSEC). Components of this work were conducted at the Penn State node of the NSF-funded National Nanotechnology Infrastructure Network.

[1] M. Zourob, S. Mohr, B. J. T. Brown, P. R. Fielden, M. B. McDonnell, and N. J. Goddard, Lab Chip **5**, 1360 (2005).
[2] X. C. Li, J. Wu, A. Q. Liu, Z. G. Li, Y. C. Seow, H. J. Huang, K. Xu, and J. T. Lin, Appl. Phys. Lett. **93**, 193901 (2008).
[3] M. M. Wang, E. Tu, D. E. Raymond, J. M. Yang, H. Zhang, N. Hagen, B. Dees, E. M. Mercer, A. H. Forster, I. Kariv, P. J. Marchand, and W. F. Butler, Nat. Biotechnol. **23**, 83 (2005).
[4] X. Mao, S.-C. S. Lin, C. Dong, and T. J. Huang, Lab Chip **9**, 1583 (2009).
[5] D. Yin, J. P. Barber, D. W. Deamer, A. R. Hawkins, and H. Schmidt, Opt. Lett. **31**, 2136 (2006).
[6] D.-H. Kim, P. K. Wong, J. Park, A. Levchenko, and Y. Sun, Annu. Rev. Biomed. Eng. **11**, 203 (2009).
[7] V. K. S. Hsiao, J. R. Waldeisen, Y. B. Zheng, P. F. Lloyd, T. J. Bunning, and T. J. Huang, J. Mater. Chem. **17**, 4896 (2007).
[8] T. J. Huang, M. Liu, L. D. Knight, W. W. Grody, J. F. Miller, and C.-M. Ho, Nucleic Acids Res. **30**, e55 (2002).
[9] E. Hecht, *Optics* (Pearson Education, Inc., San Francisco, 2002), pp. 159–161.
[10] X. Heng, D. Erickson, L. R. Baugh, Z. Yaqoob, P. W. Sternberg, D. Psaltis, and C. Yang, Lab Chip **6**, 1274 (2006).
[11] X. Cui, L. M. Lee, X. Heng, W. Zhong, P. W. Sternberg, D. Psaltis, and C. Yang, Proc. Natl. Acad. Sci. U.S.A. **105**, 10670 (2008).
[12] J. Wu, X. Cui, L. M. Lee, and C. Yang, Opt. Express **16**, 15595 (2008).
[13] A. H. J. Yang, S. D. Moore, B. S. Schmidt, M. Klug, M. Lipson, and D. Erickson, Nature (London) **457**, 71 (2009).
[14] J. T. Blakely, R. Gordon, and D. Sinton, Lab Chip **8**, 1350 (2008).
[15] W. Z. Song, A. Q. Liu, S. Swaminathan, C. S. Lim, P. H. Yap, and T. C. Ayi, Appl. Phys. Lett. **91**, 223902 (2007).
[16] J. Shi, X. Mao, D. Ahmed, A. Colletti, and T. J. Huang, Lab Chip **8**, 221 (2008).
[17] P. Y. Chiou, A. T. Ohta, and M. C. Wu, Nature (London) **436**, 370 (2005).
[18] J. Shi, D. Ahmed, X. Mao, S.-C. S. Lin, and T. J. Huang, Lab Chip **9**, 2890 (2009).
[19] J. Shi, H. Huang, Z. Stratton, Y. Huang, and T. J. Huang, Lab Chip **9**, 3354 (2009).
[20] Z. Wu, A. Q. Liu, and K. Hjort, J. Micromech. Microeng. **17**, 1992 (2007).
[21] H. Schmidt and A. R. Hawkins, J. Micromech. Microeng. **4**, 3 (2008).
[22] A. R. Hawkins and H. Schmidt, J. Micromech. Microeng. **4**, 17 (2008).
[23] N. Chronis, G. Liu, K.-H. Jeong, and L. Lee, Opt. Express **11**, 2370 (2003).
[24] H. Ren and S. T. Wu, Opt. Express **15**, 5931 (2007).
[25] H. Ren, D. Fox, P. A. Anderson, B. Wu, and S. T. Wu, Opt. Express **14**, 8031 (2006).
[26] L. Pang, U. Levy, K. Campbell, A. Groisman, and Y. Fainman, Opt. Express **13**, 9003 (2005).
[27] A. Werber and H. Zappe, Appl. Opt. **44**, 3238 (2005).
[28] S. W. Lee and S. S. Lee, Appl. Phys. Lett. **90**, 121129 (2007).
[29] S. Kuiper and B. H. W. Hendriks, Appl. Phys. Lett. **85**, 1128 (2004).
[30] L. Dong, A. K. Agarwal, D. J. Beebe, and H. Jiang, Nature (London) **442**, 551 (2006).
[31] J. Godin, V. Lien, and Y. H. Lo, Appl. Phys. Lett. **89**, 061106 (2006).
[32] D. Y. Zhang, V. Lien, Y. Berdichevsky, J. Choi, and Y. H. Lo, Appl. Phys. Lett. **82**, 3171 (2003).
[33] X. Mao, J. R. Waldeisen, B. K. Juluri, and T. J. Huang, Lab Chip **7**, 1303 (2007).
[34] S. K. Y. Tang, C. A. Stan, and G. M. Whitesides, Lab Chip **8**, 395 (2008).
[35] C. Song, N. T. Nguyen, S. H. Tan, and A. K. Asundi, Lab Chip **9**, 1178 (2009).
[36] X. Mao, S.-C. S. Lin, M. I. Lapsley, J. Shi, B. K. Juluri, and T. J. Huang, Lab Chip **9**, 2050 (2009).
[37] H. Huang, X. Mao, S.-C. S. Lin, B. Kiraly, Y. Huang, and T. J. Huang, Lab Chip **10**, 2387 (2010).
[38] Y. N. Xia and G. M. Whitesides, Annu. Rev. Mater. Sci. **28**, 153 (1998).
[39] J. J. Shi, Z. Stratton, S. C. S. Lin, H. Huang, and T. J. Huang, Microfluid. Nanofluid. **9**, 313 (2010).